ELSEVIER

Journal of Non-Crystalline Solids 192&193 (1995) 456–462

JOURNAL OF NON-CRYSTALLINE SOLIDS

Energy-filtered electron diffraction study of vitreous and amorphized silicas

L.C. Qin, L.W. Hobbs *

Department of Materials Science and Engineering, Massachusetts Institute of Technology, Cambridge, MA 02139, USA

Abstract

Radial distribution functions deduced from energy-filtered electron diffraction data have been obtained for vitreous silica, neutron-amorphized quartz, ion-amorphized quartz and electron-amorphized quartz, cristobalite and tridymite. Measurable differences in short-range and medium-range structure exist among these six forms of metamict silica.

1. Introduction

Silicas (SiO_2) adopt a range of polymorphic structures comprising the crystalline polymorphs quartz, cristobalite, tridymite, etc., and aperiodic forms generated by melt-quenching, thermal oxidation or vapor deposition. In addition, the crystalline polymorphs undergo a crystalline-to-amorphous (metamict) transformation under electron [1], neutron [2] and ion [4] irradiation at high fluences. Although all final products appear to be homogeneous and aperiodic, differences in structure at the atomic level remain to be elucidated.

Electrons are scattered more strongly by matter than X-rays or neutrons. This property allows diffraction analysis of micro-volumes of solids with good statistics and renders electrons a unique probe in the study of thin films or the small volumes amorphized by electron or ion irradiation. However, owing to the high inelastic scattering cross-section contributing to a strong diffuse background, a process to remove the inelastically scattered electrons from collected diffraction intensity data (energy-filtering) is necessary for the deduction of radial distribution functions (RDFs).

In this paper, an electron-amorphographic investigation of the atomic structures of vitreous silica, electron-metamict, neutron-metamict and ion-metamict quartz, and electron-metamict cristobalite and tridymite is reported. RDFs are deduced from energy-filtered electron diffraction (EFED) data from these various aperiodic states of silica.

2. Experimental procedures and theory

Hydrothermally grown single crystals of α-quartz were obtained from the Sawyer Research Company, Eastlake, OH. Electron microscope specimens were prepared by cutting the crystal boule into thin slices 3 mm in diameter; these were mechanically polished and ion milled to reduce the central portion to electron transparency. Electron microscope specimens of vitreous silica (v-SiO_2), obtained in the form of rods of Suprasil W, were prepared by the same method.

* Corresponding author. Tel: +1-617 253 6835. Telefax: +1-617 252 1020. E-mail: hobbs@mit.edu.

SSDI 0022-3093(95)00450-5

Cristobalite (collection catalog number 128694) and tridymite (collection catalog number 119881) crystals in the form of powders were obtained from the Harvard Mineralogical Museum. Electron microscope specimens of these materials were made by first dispersing the powders into methanol, then collecting the powders on copper grids covered by holey carbon films.

The metamict transformation was induced by irradiating material thinned to electron transparency in situ in a scanning transmission electron microscope (STEM) with 100 keV electrons at room temperature. The total electron fluence required to amorphize quartz crystals is about 10^{25} electrons/m^2, while smaller fluences are required to amorphize cristobalite and tridymite. Neutron-metamict quartz was obtained by irradiating quartz crystals with fission-reactor neutrons (~ 1 MeV) to a fluence of 1.5×10^{24} neutrons/m^2 near room temperature, sufficient to render quartz fully aperiodic as adjudged by transmission electron microscopy and diffraction. Quartz was also ion-implanted with 150 keV Si^+ ions to a fluence of 2×10^{21} Si^+/m^2, resulting in an amorphized layer extending some 510 nm from the surface, with a peak excess Si content of $< 2\%$ in the stopping zone.

Energy-filtered electron diffraction data were acquired in a VG HB5 STEM equipped with a serial energy-loss spectrometer operating at 100 keV, using an energy window of about 2 eV in width centered on zero energy loss [3,4].

In a binary system, such as SiO_2, consisting of silicon and oxygen atoms, the experimental reduced RDF deduced from elastically-scattered electron intensity data is

$$
\begin{aligned}
g_e(r) &= 4\pi r^2[\rho_e(r) - \bar{\rho}_e] \\
&= 8\pi r \int_0^\infty qS(q)\sin(2\pi qr)M(q)\,\mathrm{d}q \\
&= 8\pi r\left\{\left[\int_0^\infty \left(\frac{f_1}{\bar{f}}\right)^2 \cos(2\pi qr)M(q)\,\mathrm{d}q\right]\right. \\
&\quad *[r(\rho_{11}(r) - \bar{\rho}_1)] \\
&\quad +2\left[\int_0^\infty \left(\frac{f_2}{\bar{f}}\right)^2 \cos(2\pi qr)M(q)\,\mathrm{d}q\right] \\
&\quad *[r(\rho_{22}(r) - \bar{\rho}_2)] \\
&\quad +2\left[\int_0^\infty \frac{f_1}{\bar{f}}\frac{f_2}{\bar{f}}\cos(2\pi qr)M(q)\,\mathrm{d}q\right] \\
&\quad \left.*[r(\rho_{12}(r) - \bar{\rho}_2)]\right\}, \qquad (1)
\end{aligned}
$$

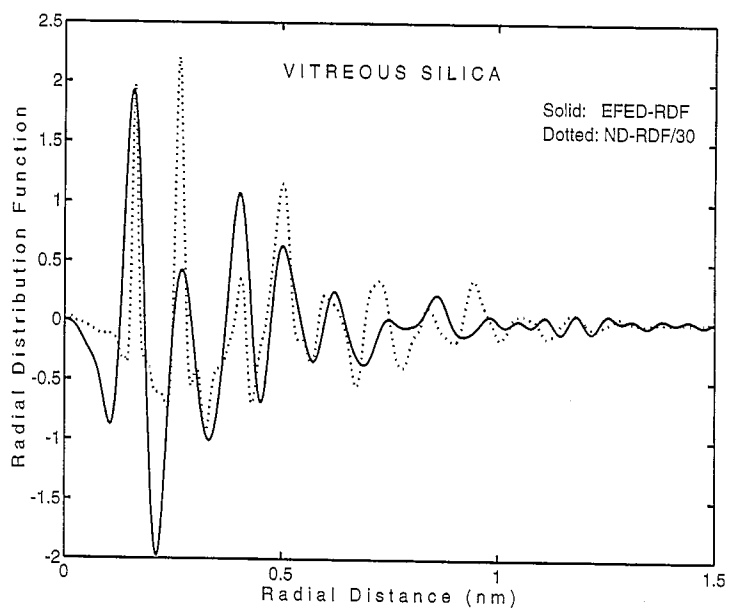

Fig. 1. Reduced radial distribution functions, $g(r)$, for vitreous silica using neutron and energy-filtered electron diffraction data. The ordinate is in units of atom/0.1 nm; $g_n(r)$ is normalized to have a first correlation peak height identical to that of $g_e(r)$.

where subscripts 1 and 2 refer to silicon and oxygen atoms, respectively; $\rho_{11}(r)$, $\rho_{22}(r)$ and $\rho_{12}(r)$ are the three independent partial radial density functions; f_1 and f_2 are the atomic scattering amplitudes; $\bar{f}$ is a sharpening function; and $M(q)$ is a modification function introduced to account for the truncation effect in experiment. The function

$$S(q) = \frac{I(q) - I(0)\,\delta_{q0}}{N_c \bar{f}^2} - \frac{1}{\bar{f}^2} \sum_{uc} f_j^2 \qquad (2)$$

is the interference function (Zernike–Prins function), in which $I(q)$ is the experimentally measurable intensity, N_c is the number of units of composition in the scattering volume, *uc* refers to the unit of composition, and the scattering vector q is defined by

$$q = 2\sin(\theta/2)/\lambda, \qquad (3)$$

where θ and λ are the scattering angle and electron wavelength, respectively.

In the present study, the sharpening function used was

$$\bar{f} = f_1 + 2f_2 \qquad (4)$$

for electron diffraction data, while the Lorch modification function [5]

$$M(q) = \frac{\sin(\pi q/q_{\max})}{\pi q/q_{\max}} \qquad (5)$$

was used in deducing reduced radial distribution functions from both electron and neutron diffraction data, where $q_{\max}$ is the maximum value for q obtained in experiment. For electron diffraction experiments [4] $q_{\max} = 16\ \text{nm}^{-1}$; this roughly corresponds to a real space resolution limit of

$$\Delta r \sim (1/q_{\max}) = 0.06\ \text{nm}. \qquad (6)$$

For the higher resolution neutron diffraction [6], $q_{\max} = 72\ \text{nm}^{-1}$.

3. Results

Fig. 1 shows a reduced RDF for v-SiO_2 derived using equation (1) from EFED data. The reduced RDF deduced from high-resolution neutron diffrac-

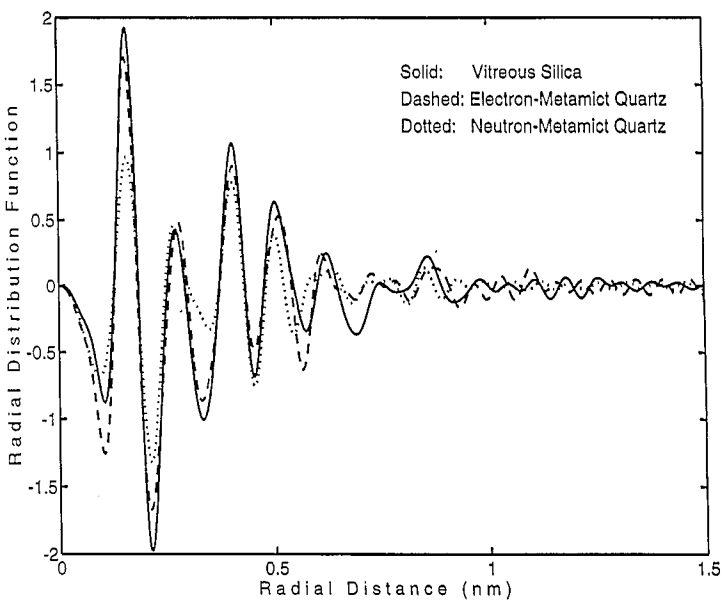

Fig. 2. Reduced radial distribution functions for vitreous silica, electron-metamict quartz and neutron-metamict quartz deduced from energy-filtered electron diffraction data. The ordinate is in units of atom/0.1 nm.

tion data [6] is also given for comparison, normalized to give the same first RDF peak height as the EFED data. For neutron diffraction, since the scattering lengths are constants ($b_1 = 0.4149 \times 10^{-14}$ m; $b_2 = 0.5804 \times 10^{-14}$ m) [7], the reduced RDF thus obtained is a linear combination of the partial RDFs:

$$\begin{aligned} g_n(r) &= 4\pi r^2[\rho_n(r) - \bar{\rho}_n] \\ &= 8\pi r \int_0^\infty q i_n(q) \sin(2\pi qr) M(q)\, dq \\ &\simeq 4\pi b_1^2\{r^2[\rho_{11}(r) - \bar{\rho}_1]\} \\ &\quad + 8\pi b_2^2\{r^2[\rho_{22}(r) - \bar{\rho}_2]\} \\ &\quad + 8\pi b_1 b_2\{r^2[\rho_{12}(r) - \bar{\rho}_2]\}. \end{aligned} \tag{7}$$

Within the poorer resolution afforded by the electron diffraction measurements, extending to only a quarter the q range of neutron diffraction studies and with reversed relative sensitivities to Si and O, the agreement is sufficiently good to provide an adequate reference for EFED-derived RDFs from metamict structures. Although all experimental RDFs have the convoluted form (1), the sharp peaks due to the short-range order in the structure are still well preserved. The peaks at 0.16 and 0.26 nm have their origin in the well-defined interatomic distances of Si–O and O–O in the constituent [SiO_4] tetrahedra in the tetrahedral network structure of vitreous silica.

Fig. 2 shows reduced RDFs for electron-metamict quartz and neutron-metamict quartz deduced from EFED data, together with the reduced RDF for v-SiO_2 for comparison. The first two peak positions in the RDFs for electron-metamict quartz and neutron-metamict quartz are unchanged, which means that the interatomic distances for the first two nearest neighbors have not been altered significantly. The Si–O (0.16 nm) and O–O (0.26 nm) bond lengths are the same as in v-SiO_2, which suggests that the basic structural unit, the [SiO_4] tetrahedron, is largely preserved in the structures of electron-metamict and neutron-metamict quartz. However, the area under the first peak in the RDF for both metamict quartz forms is smaller than that for v-SiO_2. This change in area could indicate a reduction of the coordination number for the Si–O connections but could also reflect increased distortion of [SiO_4] tetrahedra, the peak broadening from which is not detectable with the resolution limitation imposed by the electron diffraction method.

Fig. 3 plots the interference function $S(q)$ (2) for vitreous silica and the three forms of metamict quartz generated. For vitreous silica, the FSDP occurs at

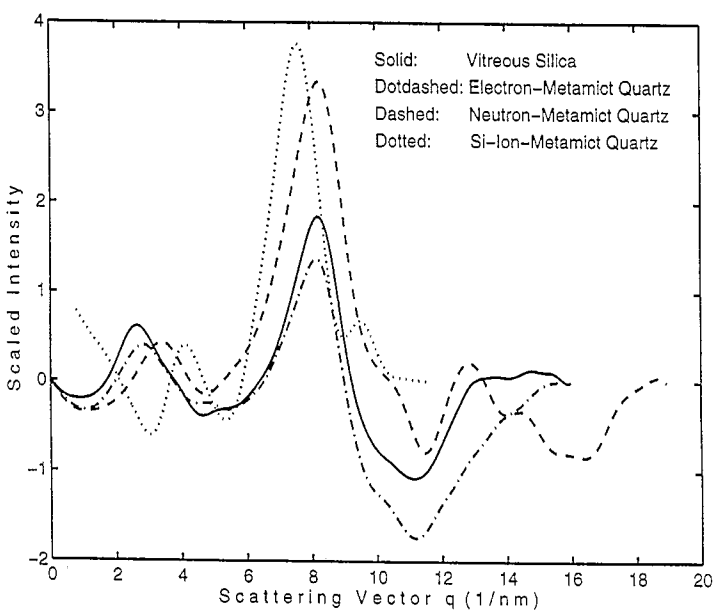

Fig. 3. Zernike–Prins function $S(q)$ (2) for vitreous silica and quartz amorphized by 100 kV electrons, fission neutrons and 150 keV Si^+ ions. The first sharp diffraction peak exhibits a progressive shift from ~ 2.4 nm^{-1} to ~ 4 nm^{-1}.

~ 2.4 nm^{-1}, corresponding to a real-space correlation distance of ~ 0.4 nm, and the radial distribution functions reconstructed from $S(q)$ are fairly insensitive to the removal of this peak, at least over the the first several real-space correlation peaks. For electron-metamict and neutron-metamict quartz, the FSDP is depressed and shifted to higher q, to ~ 2.5 nm^{-1} for electron-irradiation and to ~ 3.5 nm^{-1} for neutron-irradiation. A very large shift (to ~ 4 nm^{-1}) is observed for quartz amorphized by Si^+ implantation.

Fig. 4 shows reduced RDFs for electron-metamict cristobalite and tridymite; the reduced RDF for electron-metamict quartz is also plotted for comparison. The first correlation peak for all three metamict forms is nearly identical, but the second peak, corresponding largely to O–O correlations, is considerably larger in metamict cristobalite and tridymite.

4. Discussion

There have been five other structural investigations of metamict silica, carried out exclusively on fast-neutron-irradiated melt quenched vitreous silica, using X-ray diffraction [5,8,9], infrared spectroscopy [9], magic-angle spinning nuclear magnetic resonance [10,11] and neutron diffraction [11]. By comparison with unirradiated vitreous silica, these studies have demonstrated a small increase in Si–O and O–O distances and a diminished and broadened first sharp diffraction peak (FSDP) at higher q, both consistent with the 2.4% increase in density attendant upon neutron irradiation [2]. A reduction in the Si–O–Si bond angle from 150.5° to 141° and the reduced longer-range density fluctuation are, in turn, consistent with a partial loss of medium-range order. None of these techniques is applicable to investigation of small volumes amorphizable by electron irradiation, nor has there been analogous study of metamict forms of the crystalline polymorphs. Some similarities in the EFED-derived RDF for the neutron-metamict quartz (Fig. 2) and that derived for neutron-irradiated vitreous silica by neutron diffraction [11] are apparent, for example, an increased contribution in the region of 0.32 nm (which Wright et al. [11] attribute to Si–O(2) correlations in the presence of the three-membered siloxane rings) and reduced longer-range density fluctuations.

The crystalline polymorphs amorphize easily under displacive irradiation because (with the exception of stishovite) the corner-sharing of their tetrahedra imparts marginal structural freedom for rearrangement [12]. For electron energies up to about 1 MeV

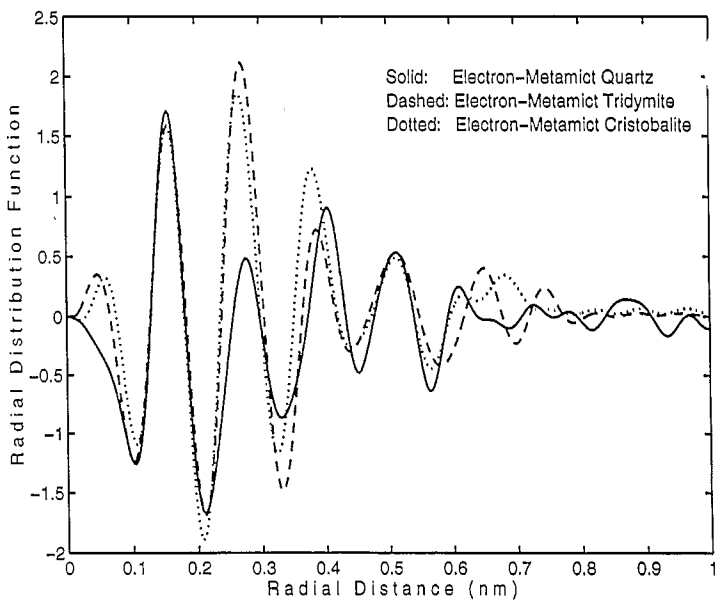

Fig. 4. Reduced radial distribution functions for electron-metamict quartz, tridymite, and cristobalite deduced from energy-filtered electron diffraction data. The ordinate is in units of atom/0.1 nm.

[13], crystalline silicas are amorphized by a principally radiolytic displacement mechanism [1] in which it has been proposed that an oxygen atom is removed from its tetrahedral site to form an E″ oxygen vacancy center and an $O^{=}_2$ interstitial peroxy linkage which comprise a close Frenkel pair. Stochastic rebonding of the damaged structure occurs when there is a high enough density of broken Si–O linkages, but the process may not achieve completeness. The small reduction in Si–O nearest-neighbor coordination number in electron-metamict quartz, inferred from the reduction in the first RDF peak areas in Fig. 1, could be accounted for by the leftover presence of some of the resulting three-coordinated Si in the metamict states, for example, $[SiO_3]$ units perhaps relaxed into a more planar form [14] while, in the ideal continuous random network structure of vitreous silica, such configurations should be absent.

The mechanism for primary change during fast-neutron irradiation – direct knock-on atomic displacements distributed in extensive collision cascades – is more likely than single radiolytic events to displace oxygen atoms to interstitial sites in the open network structure of metamict quartz, well-removed from the initial Si–O–Si bonding connections; a possible reduction in the average coordination number about Si for the neutron-metamict quartz inferred from Fig. 1, could support this interpretation.

While there has been no previous structural study of metamict crystalline polymorphs, Konnert et al. [15] have constructed RDFs for crystalline quartz, cristobalite and tridymite and noted that the experimental RDF for vitreous silica bears a strong resemblance to that of tridymite, the structure whose density is also closest to the density of metamict silica. Of the crystalline polymorphs, tridymite and cristobalite have the most open structures and contain only six-membered rings (six-rings), while quartz is over 14% denser because it additionally contains many eight-rings [16]. The radiolytic damage mechanism [1] is likely to operate identically in each of these precursor polymorphs, but tridymite and cristobalite transform rapidly and seemlessly on an atomic scale [12,17], while quartz transforms more slowly with the formation of strained amorphous nuclei [1].

The difference can be understood topologically [12] if one assumes a metamict structure – like cristobalite or tridymite – dominated by six-rings. An $[SiO_4]$ tetrahedron in the network structure of quartz has 30 third-network neighbors, while a network dominated by six-rings will, like tridymite and cristobalite, have only 24 or 25; the transformation in quartz, therefore, involves considerable restructuring at third-network neighbor distances, thus favoring a nucleation-and-growth transformation morphology to minimize strain energy. The structure of the electron-metamict quartz product appears to differ from that of metamict tridymite or the metamict cristobalite products (which are themselves similar, Fig. 4), as evidenced by the respective strengths of the RDF peak at 0.26 nm and the positions of the peak around 0.4 nm. The internal pressure in the strained transformation nuclei in quartz is high [18] and may influence the resulting metamict structure, while the less-constrained environment for tridymite or cristobalite may differently affect the subsequent network reconstruction following the radiolytic bond breakage.

Beyond the regime of short-range order, extending to a spatial range of about 0.3 nm for this study, RDFs are no longer directly interpretable in terms of structural units. The differences in this medium-range structural domain are, nonetheless, measurable and significant but best understood topologically [19]. In diffraction space, the FSDP is customarily taken as a signature of this medium-range structure [20]. The FSDPs from the metamict silicas examined (Fig. 3) compare with that for the unirradiated vitreous silica in parallel fashion to evolution of the FSDP during high-dose neutron irradiation of vitreous silica [11]: the FSDP decreases in intensity, marginally broadens and shifts to higher q values. The significantly larger shift for neutron-metamict quartz compared with electron-metamict quartz probably reflects the differences in network reconstruction following single-displacement and cascade disorder. The still larger shift and anomalous width for Si ion-implanted quartz undoubtedly reflect the presence of excess silicon in the implantation zone. The relationship derived between topological ring structure and the FSDP from various aperiodic silicas is discussed elsewhere [21].

The authors are grateful to Dr D.L. Griscom for providing the v-SiO_2 material, Dr Carl Francis for

loaning the cristobalite and tridymite samples used in this study and Dr A.J. Garratt-Reed for assistance in acquiring the EFED data. This project is financially supported by the US Department of Energy, Office of Basic Energy Sciences, through grant DE-FG02-89ER45396.

References

[1] L.W. Hobbs and M.R. Pascucci, J. Phys. (Paris) 41 (Colloque C6) (1980) 237.
[2] M.C. Wittels and F.A. Sherrill, Phys. Rev. 93 (1954) 1117.
[3] L.C. Qin, A.J. Garratt-Reed and L.W. Hobbs, in: Proc. 50th Ann. Meeting of the Electron Microscopy Society of America, ed. G.W. Bailey, J. Bentley and J.A. Small (San Francisco Press, 1992) p. 350.
[4] L.C. Qin, ScD thesis, MIT (1994).
[5] E. Lorch, J. Phys. (Paris) C2 (1969) 229.
[6] A.C. Wright, J. Non-Cryst. Solids 123 (1990) 129.
[7] G.E. Bacon, Neutron Diffraction, 3rd Ed. (Clarendon Press, Oxford, 1975).
[8] I. Simon, J. Am. Ceram. Soc. 40 (1957) 150.
[9] A.J. Leadbetter and A.C. Wright, Phys. Chem. Glasses 18 (1977) 79.
[10] S.L. Chan, L.F. Gladden and S.R. Elliott, J. Non-Cryst. Solids 106 (1988) 413.
[11] A.C. Wright, B. Bachra, T.M. Brunier, R.N. Sinclair, L.F. Gladden and R.L. Portsmouth, J. Non-Cryst. Solids 150 (1992) 69.
[12] L.W. Hobbs, Nucl. Instrum. Meth. B91 (1994) 30; J. Non-Cryst. Solids 182 (1995) 27.
[13] H. Inui, H. Mori, T. Sakata and H. Fujita, J. Non-Cryst. Solids 116 (1990) 1.
[14] A.H. Edwards and W.B. Fowler, J. Phys. Chem. Solids 46 (1985) 841.
[15] J.H. Konnert, P. D'Antonio and J. Karle, J. Non-Cryst. Solids 53 (1982) 135.
[16] C.S. Marians and L.W. Hobbs, J. Non-Cryst. Solids 124 (1990) 242.
[17] L.C. Qin, in Proc. 51st Ann. Meeting of the Microscopy Society of America, ed. G.W. Bailey and C.L. Reider (San Francisco Press, 1993) p. 1102.
[18] K. Tanimura, T. Tanaka and N. Itoh, Phys. Rev. Lett. 51 (1983) 423.
[19] L.W. Hobbs, these Proceedings, p. 79.
[20] S.R. Elliott, Nature 354 (1991) 445.
[21] L.C. Qin and L.W. Hobbs, Mater Res. Soc. Symp. Proc. 373 (1995) 341.